Indian Journal of Chemical Technology
Vol. 20, November 2013, pp. 371-379

Cadmium removal using waste residue generated after recovery of base metals from manganese nodules

N S Randhawa[1], N N Das[2] & R K Jana[1,*]

[1]Metal Extraction & Forming Division, CSIR-National Metallurgical Laboratory, Jamshedpur 831 007, India
[2]PG Department of Chemistry, North Orissa University, Baripada 757 003, India

Received 29 May 2012; accepted 22 May 2013

The laboratory scale investigations on Cd^{2+} removal characteristics of waste manganese leach residue (***w***MNR), generated by reduction roasting – ammonia leaching of manganese nodules have been studied. Adsorption studies show rapid kinetics of Cd^{2+} adsorption. About 90% of total Cd^{2+} adsorption occurs within 15 min contact time and equilibrium is attained within 30 min. The quantity of Cd^{2+} adsorption increases with increase in leached residue dose but decreases with increase in initial Cd^{2+} concentrations. The adsorption is found to be dependent on initial ***p***H of Cd^{2+} solution, which increases with increase in initial ***p***H of the solution. Adsorption data are satisfactory fitted to the Langmuir isotherms. The loading capacity of Cd^{2+}on leached residue calculated from Langmuir data is 32.26 mg g^{-1} at ***p***H 5.5 and 303 K, which improves to 38.17 mg g^{-1} at 323 K. Pseudo second-order kinetics is applicable for the Cd^{2+} adsorption. Thermodynamic studies indicate spontaneous (ΔG^0= -3.88, -5.04 and -6.0 kJ mol^{-1} at 303, 313 and 323 K respectively) and endothermic (ΔH^0= 28.3 kJ mol^{-1}) nature of adsorption. The activation energy for Cd^{2+} adsorption onto ***w***MNR is calculated to be 50.76 – 65.14 kJ $mole^{-1}$, suggesting chemisorption type adsorbate-adsorbent interaction.

Keywords: Adsorption, Cadmium, Chemisorption, Manganese nodules, Manganese nodules leach residue

The surface water bodies on the earth are often polluted by the effluents from various types of industries. Heavy metals present in these effluents, when discharged untreated, are threat to ecosystem. These metals are non-biodegradable and tend to accumulate in living organisms, causing various life threatening disorders. Among the toxic heavy metals, mercury, lead and cadmium are known as the highly toxic ones, due to their major impact on the environment[1]. The toxic and harmful effects of cadmium to human body system are very well known[2,3]. Cadmium as a pollutant is found in discharges from electroplating, alkaline batteries, paints, plastics and paper manufacturing industries[4]. Among the important technologies available for remediation of cadmium contaminated effluents, adsorption technique has been viewed as most attractive due to factors like simple operation, effectiveness, etc[5]. In addition, many adsorption techniques regenerate the adsorbent and reduce the operational cost. The key factor for the selection of an adsorbent lies with its effectiveness and most importantly its cost. Apart from much studied adsorbents like activated carbon, bio-sorbents based on agriculture (stems, peals, husks, shells, leaves, etc.), agro-industries waste materials have also been tried for the removal of cadmium from waste water[5]. Metallic oxides (Fe, Mn and Al), especially of waste category, are of much interest due to their effectiveness towards remediation of heavy metals from contaminated aqueous bodies[5].

Residues generated after hydrometallurgical treatment of manganese nodules or polymetallic sea nodules contain oxides/oxy-hydroxides of Fe, Mn, Al and Si with a reasonable porosity and surface area. These residues have been utilized as an effective adsorbent for a variety of species[6-8]. The present study is aimed at investigating the sorption characteristics of residue, generated in the reduction–roast ammoniacal leaching of manganese nodules, for the removal of Cd^{2+} from its aqueous solution. Emphasis has been given on characterization of leached residue of cadmium, its regeneration after adsorption and the underlying mechanism of adsorption.

Experimental Procedure

Materials

The adsorbent material, i.e. leached manganese nodule residue (MNR), was obtained from large scale trial of reduction roasting - ammoniacal leaching of manganese nodules at CSIR-National Metallurgical

*Corresponding author.
E-mail: rkjana@nmlindia.org

Laboratory, Jamshedpur, India. The MNR was air-dried for several days, mixed thoroughly and stored in air-tight bottles for characterization and further use. To remove the entrapped leach liquors, MNR was washed with deionised water with 1:10 solid-to-liquid ratio and stirred for 2 h. The washed manganese nodule residue (***w***MNR) was separated by filtration, washed with deionised water, air-dried for several days and then used for subsequent characterization and adsorption studies.

The synthetic stock solution (1000 mg L^{-1}) was prepared by dissolving $Cd(NO_3)_2$ in deionised water and the solution was made slightly acidic by adding a few drops of HNO_3 to prevent hydrolysis of the solution. Solutions of 0.01 M HNO_3 and 0.01 M NaOH were used for ***p***H adjustment. 0.1N KNO_3 was used to maintain the ionic strength in the adsorption experiments. All the chemicals were Merck™- AR grade. The water processed by Milli-Q™ system was used for all the experimental and analytical purposes.

Methods

Sample characterization

The chemical composition of leached manganese nodules residue of ***w***MNR was determined by standard conventional wet and instrumental methods. Surface area measurement was conducted using Quantachrome® (Model: 4000E) surface area analyser (Nova Instruments, USA). Size analysis was carried out in Malvern Mastersizer after ultrasonic liberation of particles. Morphology of ***w***MNR particles was examined in a Hitachi-S3400N scanning electron microscopy (SEM, Japan) operating at 15 kV. The ***w***MNR particles for SEM studies were mounted on metal stubs with double-side adhesive, and coated in vacuum using an Emitech K575X sputter coater. X-ray diffraction patterns were recorded on a Siemens D500 X-ray diffractometer using Cu ***K***α radiation. FTIR spectra employing the KBr disc technique were collected using a ThermoNicolet 870 FTIR spectrophotometer in the absorption mode, averaging 32 scans at a resolution of 4 cm^{-1}.

Adsorption kinetics experiments

For kinetic studies typically 50 mL of Cd^{2+} solution at desired concentration with appropriate amount of adsorbent in 100 mL stoppered conical flask was taken. The required ***p***H was adjusted and it was then mechanically shaken (120 strokes min^{-1}) using a water bath shaker, maintained at temperatures 303, 313 and 323 K as per requirement. Samples were withdrawn at certain time interval and the solid adsorbent was separated by filtration. The remaining cadmium in the filtrate was analyzed by atomic absorption spectrometer (Perkin Elmer, model: A Analyst 400). The amount of cadmium per gram of the ***w***MNR [$\boldsymbol{Q_t}$ (mg g^{-1})] was calculated using the following equation:

$$\boldsymbol{Q_t} = \frac{(\boldsymbol{C_o} - \boldsymbol{C_t})\ \boldsymbol{V}}{\boldsymbol{w} \times 1000} \quad \ldots (1)$$

where $\boldsymbol{C_o}$ and $\boldsymbol{C_e}$ are the initial and final cadmium ion concentration (mg L^{-1}) in solution respectively; ***V***, the volume of solution in mL; and ***w***, the mass of sorbent in gram.

Equilibrium experiments

The equilibrium adsorption experiments were carried out to investigate the effect of various parameters, such as ***p***H of the adsorbate solution (3-8), initial cadmium concentration (5-100 mg L^{-1}), adsorbent dose (0.25-5.0 g L^{-1}) and temperature (303-323 K) under fixed equilibration time obtained by kinetic experiments. For all the equilibrium experiments, 50 mL of solution in100 mL stoppered conical flask was mechanically shaken (120 strokes min^{-1}) using a water bath shaker. Each experiment was duplicated under identical conditions.

Results and Discussion

Adsorbent characterization

Detailed chemical analysis of manganese nodule residue (MNR) and washed residue (***w***MNR) is given in Table 1. The ***p***H_{pzc} and specific gravity are 6.5 and 3.1 respectively. The bulk surface area of ***w***MNR

Table 1 ─ Chemical analysis of manganese nodule residue (MNR) and washed residue (***w***MNR).

Element/radical	Chemical composition, % by mass	
	MNR	***w***MNR
Mn(T)[a]	25.66	26.11
Mn^{2+}	14.02	13.71
Mn^{3+}	4.87	4.92
Mn^{4+}	6.77	7.22
Fe	9.92	10.19
SiO_2	15.28	16.44
Al_2O_3	3.53	3.54
S	0.37	0.08
NH_4^+	0.30	Not found
Co	0.035	0.039
Ni	0.07	0.05
Cu	0.26	0.13
Moisture	8.96	6.18
LOI[b]	18.85	17.01

[a]The values for Mn^{2+} , Mn^{3+} and Mn^{4+} represent the respective wt% of the total manganese content in the samples.
[b]Loss in weight on ignition.

obtained by BET isotherm of N_2 adsorption is 66.7 $m^2 g^{-1}$. Particle size analyses of ***w***MNR reveals very fine granulometry with mean particle diameters (d_{50}) of 17.8 µm. The morphology of ***w***MNR particles under scanning electron microscope is shown in Fig. 1(a), which reveals irregular shapes of ***w***MNR particles, congregated moderately. The point analysis by EDX also reveals the Mn and Fe as major constituent. The weight % of Si is found to be very less presumably due to the reason that Si phases containing particle are finer and partially covered by Mn and Fe containing phases.

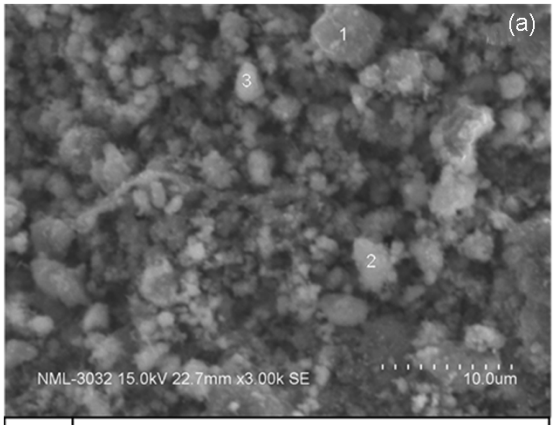

EDX point	Weight %						
	C	O	Mg	Si	Ca	Mn	Fe
1	0.00	3.86	0.00	2.23	2.65	48.44	42.83
2	0.00	5.29	0.06	0.96		93.68	
3	0.57	4.61	0.00	1.33	4.21	89.29	

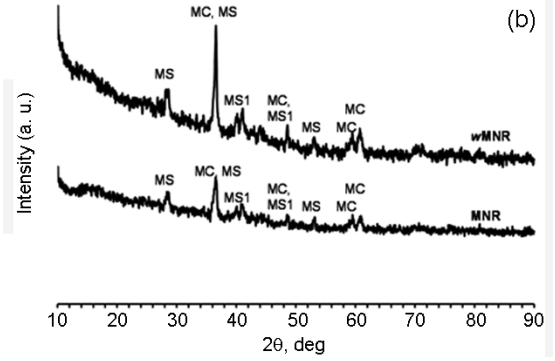

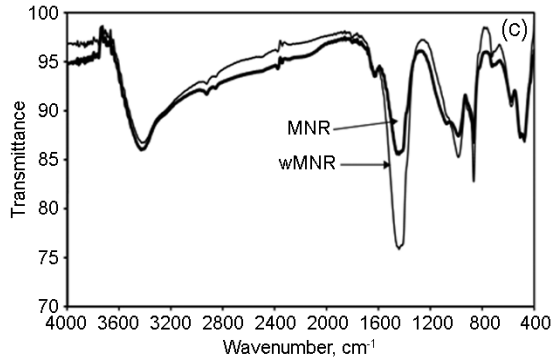

Fig. 1 ─ Characterisation of MNR and ***w***MNR (a) SEM image and EDX point analysis of ***w***MNR, (b) powder X-ray diffraction patterns. [Abbreviations associated with the patterns MC - $MnCO_3$, MS – Mn_2SiO_4, MS1 – $Mn_2SiO_3(OH)_2.H_2O$], and (c) FTIR spectra

The X-ray diffraction patterns of air-dried MNR and ***w***MNR are depicted in Fig. 1(b). The prominent peaks are assigned to mainly three phases, namely $MnCO_3$, Mn_2SiO_4 and $Mn_2SiO_3(OH)_2.H_2O$. On washing with distilled water, no changes in the position of the characteristic peaks in ***w***MNR are observed from those of MNR. The FTIR spectra of air-dried MNR and ***w***MNR are presented in Fig. 1(c). The broad absorption band at 3445 cm^{-1} and the band of moderate intensity at 1650 cm^{-1} in the spectra of both the samples may be attributed to O–H stretching and vibration bending modes[9]. The absorption bands in MNR at 1470, 1070 and 870 cm^{-1} are mainly attributed to the ν(C–O) and δ(OCO) vibrations of the carbonate ion respectively[9,10]. This denotes the formation of $MnCO_3$ in MNR during the reduction–roasting–leaching cycle for the processing of manganese nodules. Positions of the majority of the bands in MNR remain unchanged after washing, except for the disappearance of the absorption band at 1072 cm^{-1}, presumably due to the loss of a small amount of loosely bound NH_3 or sulphate on washing[6]. The sulphate is most likely generated from the impurities in the fuel oil employed during the reduction–roasting of manganese nodules.

Effect of *p*H on adsorption of Cd^{2+} onto wMNR

The solution ***p***H is an important parameter which affects adsorption of heavy metal ions. The adsorption of cadmium was studied over the ***p***H range ~ 3–8 and the results are shown in Fig. 2. It is observed that the adsorption of Cd(II) increases with the increase in ***p***H.

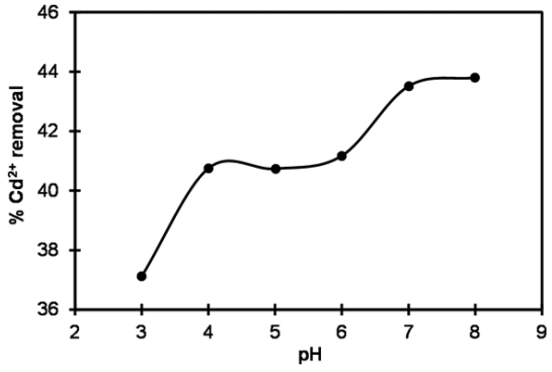

Fig. 2 ─ Effect of ***p***H on Cd^{2+} adsorption on ***w***MNR [[Cd(II)] 50 mg L^{-1}, temperature 303 K, ***w***MNR 1000 mg L^{-1} and time 1 h]

This may be attributed to competitive binding between H_3O^+ ions and Cd(II) ions at the ***w***MNR surface. As ***p***H value increases, the competing effect of H_3O^+ ions decreases and the positively charged Cd^{2+} ions get adhere to free binding sites. The other important factor, which might contribute to the higher adsorption of metal ions with increased ***p***H, is the $\boldsymbol{p}H_{pzc}$ of ***w***MNR. When the solution ***p***H exceeded $\boldsymbol{p}H_{pzc}$, the metal species are more easily attracted by the negatively charged surface of adsorbent, favoring accumulation of metal species on the surface and thus promoting adsorption. In addition to that, Cd^{2+} uptake is almost unchanged in the ***p***H range of 4-6, independent of surface charge. However, when solution ***p***H increases above the $\boldsymbol{p}H_{pzc}$ of ***w***MNR, i.e. 6.5, there is sudden rise in adsorption of Cd^{2+}. In addition to this, increase in Cd^{2+} adsorption may be partly attributed to the formation of different hydroxo species with rise in solution ***p***H. Based on the hydrolysis constants of different metal ions[11,12] as defined in the following equation, the ionic species of Cd will depend upon the ***p***H of the solution, as shown below:

$$M^{2+} + \boldsymbol{n}H_2O \rightarrow M(OH)_{\boldsymbol{n}}^{2-\boldsymbol{n}} + \boldsymbol{n}H^+ \quad \ldots (2)$$

where M stands for metal.

The Cd(II) speciation diagram[6] shows that the dominant Cd(II) species up to ***p***H 7.5 is Cd^{2+}. The $Cd(OH)_2$ exists at ***p***H > 9.5 and $Cd(OH)^+$ exists in the ***p***H range 7.5-9.5. Since maximum adsorption for Cd^{2+} is achieved at ***p***H ~ 7, it may safely be stated that the removal of cadmium is mostly due to adsorption and not precipitation.

Effect of *w*MNR dose on Cd^{2+}adsorption

Adsorption of Cd^{2+} with varying adsorbent dose, carried out to assess the effect of adsorbent on Cd^{2+} removal, is presented in Fig. 3. The results show that the equilibrium concentration ($\boldsymbol{C_e}$) of Cd^{2+} decreases with increase in the weight of ***w***MNR, which is 40 mg L^{-1} for 0.25 g L^{-1} ***w***MNR and lowered to 17 mg L^{-1} for 5.0 g L^{-1} of ***w***MNR addition. Increase in ***w***MNR dose provides higher surface area and active sites for adsorption of Cd^{2+} and ultimately is responsible for more uptake of Cd^{2+}.

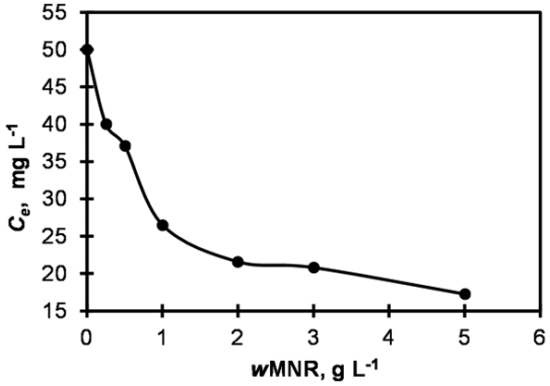

Fig. 3 — Effect of weight of ***w***MNR on Cd^{2+} adsorption [[Cd(II)] 50 mg L^{-1}, temperature 303 K, time 1 h, ***p***H 5.5]

Effect of time and initial concentration on adsorption

The time course of Cd^{2+} adsorption onto ***w***MNR at varying initial concentration is given in Fig. 4(a). The Cd^{2+} removal at equilibrium is 64, 46, 30 and 34% for 25, 50, 75 and 100 mg L^{-1} initial Cd^{2+} respectively. For a fixed dose of adsorbent the decrease in adsorption with increasing Cd^{2+} concentration is primarily due to availability of limited number of site for adsorption. Although the percentage of Cd^{2+} adsorption decreases with increase in its initial concentration, the overall uptake increases progressively. It is apparent from Fig. 4(a) that cadmium adsorption is relatively fast during initial period, more than 85-90% of the total adsorption

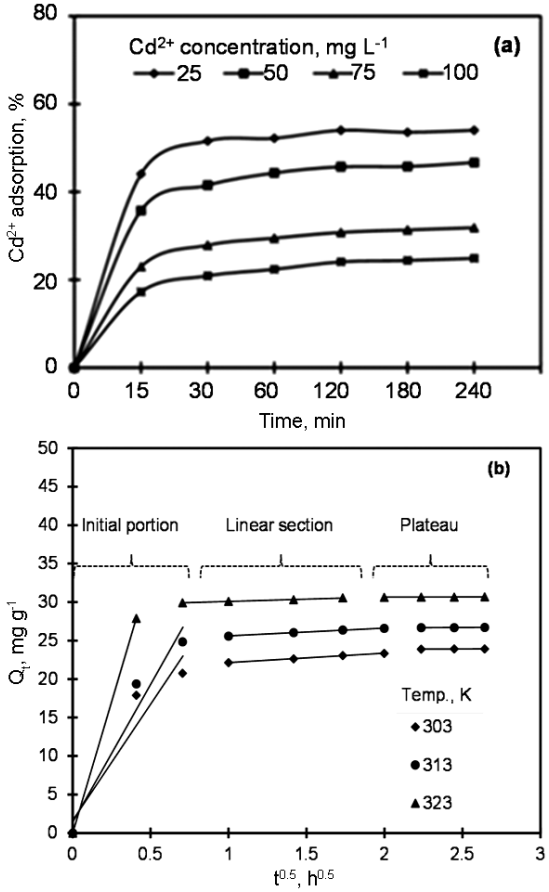

Fig. 4 — (a) Effect of time and initial concentration on Cd^{2+} adsorption onto ***w***MNR and (b) Intraparticle diffusion plots for Cd^{2+} adsorption ***w***MNR at different temperatures

takes place within 15 min and thereafter it slows down to attain the equilibrium at ~ 30 min. The equilibrium time obtained from present studies is applicable for $C_o \leq 100$ mg L^{-1}. This relatively high adsorption rate with lower equilibrium time has great practical importance, which is favorable in column or continuous operation, where the contact time between the metal solution and the sorbent is generally short. Some of the other systems are reported to have equilibrium achieved between 2 h and 72 h[13-15]. The short equilibrium adsorption time between 15 min and 30 min is reported for PEI-coated silica gel and ligand-modified gel beads[16,17]. Even shorter equilibrium time 2-10 min is obtained when sawdust is employed in the removal of Cd^{2+} ions[18,19].

Adsorption kinetics models

Kinetics and the equilibrium of adsorption are the two important factors for the evaluation of adsorption efficiency of an adsorbent. The adsorption kinetic mechanism is evaluated using two conventional models, namely the pseudo first-order[20] and the pseudo second-order[21] equations, as shown below:

$$\ln(q_e - q_t) = \ln q_e - k_1 . t \quad \ldots (3)$$

$$\frac{t}{q_t} = \frac{1}{k_2 q_e^2} + \frac{1}{q_e t} \quad \ldots (4)$$

where q_e and q_t (mg g^{-1}) are the adsorption capacities at equilibrium and at time t (min) respectively. The value of k_1 is derived experimentally from the slope of the linear plots of log ($q_e - q_t$) versus t. The k_2 is the rate constant for pseudo second-order adsorption (g mg^{-1} min^{-1}) and $k_2 q_e^2$ or h (mg g^{-1} min^{-1}) is the initial adsorption rate. The values of $1/k_2 q_e^2$ and $1/q_e$ are derived experimentally from the intercept and slope of the linear plots of t/q_t versus t, which eventually leads to values of k_2 and $q_{e\ (cal.)}$. The rate constants and other parameters of pseudo first-order and pseudo second-order are given in Table 2. The good agreement between model fit and experimentally observed equilibrium adsorption capacity in addition to the large correlation coefficients suggests that cadmium adsorption follows pseudo second-order kinetics. It is interesting to note that value of rate constant (k_2) at particular temperature increases by factor of 2 when C_o is doubled. However, this is valid for $C_o \leq 50$ mg L^{-1}. It is also notable that for each 10^oC increment of solution temperature, at fixed C_o, the rate constant (k_2) is increased by factor of 1½-3.

The kinetic data is also fitted in to the intraparticle diffusion model, expressed with the following Eq. (5), given by Weber and Morris[22]. According to this model, the uptake varies almost proportionately with $t^{½}$ rather than with the contact time t.

$$q_t = k_{id} . t^{½} \quad \ldots (5)$$

where q_t is the amount of metal ions adsorbed at time t (mg g^{-1}); and k_{id}, the intraparticle diffusion rate constant (mg g^{-1} $min^{-½}$). Plots of q_t versus $t^{½}$ are shown in Fig. 4(b). Each plot in Fig. 4(b) comprises three distinct sections, namely initial plot or steep-sloped portion represents the bulk diffusion or exterior adsorption rate which is very high, the subsequent linear portion is attributed to the intraparticle diffusion and plateau portion represents

Table 2 — Adsorption kinetic model rate constants for Cd^{2+} adsorption on *w*MNR at different temperatures

Temp. K	C_o mg L^{-1}	q_e exp. mg g^{-1}	Pseudo first-order			Pseudo second-order			
			k_1 min^{-1}	q_e cal mg g^{-1}	r_1^2	k_2 g mg^{-1} min^{-1}	q_e cal mg g^{-1}	h mg g^{-1} min^{-1}	r_2^2
303	25	17.01	0.006	5.84	0.978	0.0039	17.15	1.17	0.994
	50	23.90	0.009	4.25	0.851	0.0079	24.04	1.60	0.999
	75	30.00	0.006	16.31	0.767	0.0016	29.85	1.42	0.992
	100	31.60	0.006	17.79	0.681	0.0037	27.10	2.72	0.998
313	25	18.86	0.020	6.35	0.985	0.0079	19.31	2.94	0.999
	50	26.68	0.016	4.45	0.923	0.011	26.95	7.92	1.000
	75	33.5	0.012	11.15	0.745	0.0049	33.73	5.59	0.999
	100	31.05	0.013	11.73	0.738	0.0073	30.40	6.76	0.999
323	25	20.75	0.023	3.7	0.923	0.013	20.96	7.16	0.999
	50	30.65	0.018	6.33	0.959	0.026	30.77	24.81	1.000
	75	36.79	0.025	11.93	0.861	0.0062	37.45	8.81	0.999
	100	36.45	0.031	11.30	0.799	0.019	36.69	24.69	1.000

the equilibrium[23]. The intraparticle diffusion constants are calculated from the slopes of the linear portion of the plots and given in Table 3. The high correlation coefficients >0.99 suggest involvement of internal diffusion in the Cd^{2+} uptake on ***w***MNR.

Adsorption activation energy

The effect of temperature on kinetics of Cd^{2+} adsorption onto ***w***MNR was further evaluated using Arrhenius equation. Arrhenius equation parameters are calculated using pseudo second-order rate constants to determine temperature independent rate parameters and adsorption type. The Arrhenius equation for calculating adsorption activation energy is expressed as:

$$k_2 = k.e^{\left(-\frac{E_a}{RT}\right)} \quad \ldots (6)$$

where k_2 is the rate constant for pseudo second-order adsorption (g mg^{-1} min^{-1}); k, the temperature-independent factor (g mg^{-1} min^{-1}); E_a, the activation energy of sorption (kJ mol^{-1}); R, the universal gas constant (8.314 J mol^{-1} K); and T, the solution temperature (K). A plot of ln k_2 versus $1/T$ yields a straight line, with slope $-E_a/R$. The values of slope (m) and intercept (c) for initial Cd^{2+} concentrations 25 mg L^{-1}, 50 mg L^{-1}, 75 mg L^{-1} and 100 mg L^{-1} are m=-6.906, -5.795, -7.138, -7.835 and c=17.24, 14.19, 17.17, 20.21 respectively. The magnitude of the activation energy is commonly used as the basis for differentiating between physical and chemical adsorption. The activation energy for Cd^{2+} adsorption onto ***w***MNR is ranged between 48.18 - 65.14 kJ mol^{-1} for different initial concentrations, suggesting that the Cd^{2+} ions are chemically adsorbed onto the ***w***MNR surface[24,25].

Adsorption isotherms

The equilibrium adsorption data are fitted into the linearized form of isotherm models proposed by following Langmuir (Eq. 7) and Freundlich (Eq. 8) models[26,27]:

$$\frac{C_e}{q_e} = \frac{1}{bQ^o} + \frac{C_e}{Q^o} \quad \ldots (7)$$

$$\ln q_e = \ln K_f + n \ln C_e \quad \ldots (8)$$

where C_e is the equilibrium concentration (mg L^{-1}); q_e, the amount adsorbed at equilibrium (mg g^{-1}); K_f, b, n, the isotherm constants; and Q^o, the adsorption maxima or adsorption capacity (mg g^{-1}).

The calculated parameter from Langmuir plot of C_e versus C_e/q_e and Freundlich plot of ln q_e versus ln C_e are given in Table 4. Langmuir model is more likely applicable due to higher correlation coefficients, suggesting possible monolayer coverage of Cd^{2+} on the surface of ***w***MNR. Further, the value of Q^o, which is a measure of adsorption capacity, increases with the rise in temperature and, therefore, the increase in uptake with temperature is expected, which is supported by the present findings (Table 4). The monolayer adsorption capacity (Q^o) calculated from slope of Langmuir plot at the temperature of 303 K is 32.26 mg g^{-1} (Table 4), which improves to 38.14 mg g^{-1} at 323 K. Analogous trend is observed with the Langmuir constant b.

Dimensionless separation factor (R_L), measure of favorability of adsorption, is calculated using the following equation:

$$R_L = \frac{1}{1 + bC_o} \quad \ldots (9)$$

where C_o is the initial metal concentration (mg L^{-1}); and b, the Langmuir parameter i.e. energy of interaction at the surface. The conditions, R_L > 1: unfavorable; R_L = 1: linear; $0 < R_L < 1$: favourable; and R_L = 0: irreversible are reported in literature[28]. The calculated values of R_L are obtained in the range 0.037-0.43, suggesting that the adsorption of Cd^{2+} on ***w***MNR is favorable and reversible.

Effect of temperature and thermodynamic evaluation

The effect of temperature on Cd^{2+} uptake by ***w***MNR is also investigated via thermodynamic evaluation of equilibrium data. The thermodynamic parameters of free energy change (ΔG^0, kJ mol^{-1}), enthalpy change (ΔH^0, kJ mol^{-1}) and entropy change (ΔS^0, J mol^{-1} K) are

Table 3 — Intraparticle diffusion coefficients and intercept values for Cd^{2+} adsorption on ***w***MNR at different temperatures

Temp., K	K_{id}	Intercept	r^2
303	1.211	20.93	0.999
313	1.028	24.57	0.995
323	0.616	29.46	0.994

Table 4 — Langmuir and Freundlich isotherm model parameters and coefficients for adsorption of Cd^{2+} on ***w***MNR

Temp. K	Langmuir isotherm			Freundlich isotherm		
	Adsorption maxima (Q_o), mg g^{-1}	Binding energy constant (b), L mg^{-1}	Regression coefficient r^2	Adsorption capacity (K_f), mg g^{-1}	Adsorption intensity $1/n$	Regression coefficient r^2
303	32.26	0.258	0.981	10.52	0.26	0.973
313	35.97	0.335	0.984	14.68	0.21	0.989
323	38.17	0.562	0.994	18.61	0.17	0.973

calculated to describe the associated thermodynamic behavior. These parameters are calculated using the following equations[23]:

$$\Delta G^o = -RT \ln K_d \quad \ldots (10)$$

$$\ln K_d = \frac{\Delta S^o}{R} - \frac{\Delta H^o}{RT} \quad \ldots (11)$$

K_d can be defined as

$$K_d = \frac{a_s}{a_e} = \frac{{}_s C_s}{{}_e C_e} \quad \ldots (12)$$

where R is the universal gas constant (8.314 J mol^{-1} K); T, the solution temperature (K); and K_d, the distribution coefficient (cm^3 g^{-1}). Also, a_s = activity of adsorbed Cd^{2+}, a_e = activity of Cd^{2+} in solution at equilibrium, γ_s = activity coefficient of adsorbed Cd^{2+}, γ_e = activity coefficient of Cd^{2+} in equilibrium solution, C_s = Cd^{2+} adsorbed on ***w***MNR (mg g^{-1}), and C_e = Cd^{2+} concentration in equilibrium solution (mg L^{-1}). K_d at different temperatures is determined by plotting ln(C_s/C_e) versus C_s (Fig. 5a) and extrapolating C_s to zero. The plot of ln K_d versus 1/T is a straight line (Fig. 5b) and from the slope and intercept the values of

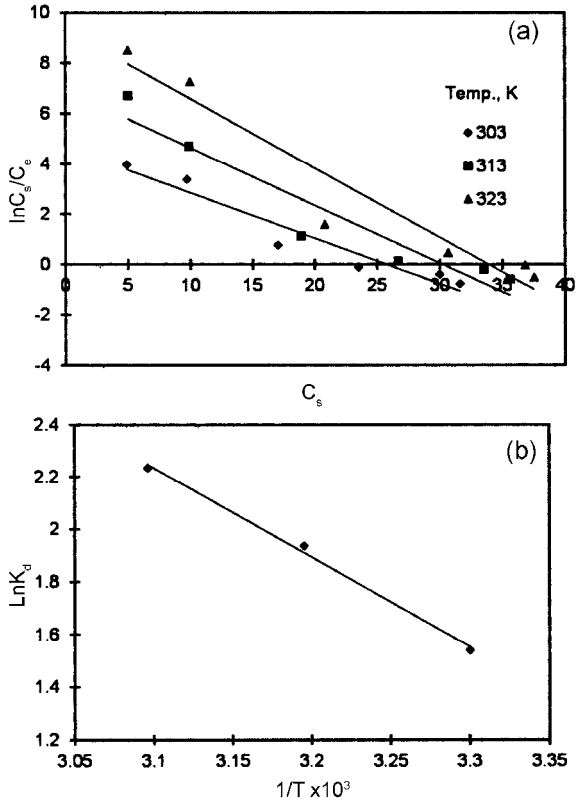

Fig. 5 — (a) Determination of distribution coefficient (K_d) and (b) Vant Hoff plot, for Cd^{2+} adsorption onto ***w***MNR

ΔS^0 and ΔH^0 respectively are calculated. The positive value of ΔH^0 (28.3 kJ mol^{-1}) confirms the endothermic nature of the overall adsorption process, which is supported by the increasing adsorption of $Cd^{2+}$with increase in temperature. The positive standard entropy change (106.25 J mol $^{-1}$ K^{-1}) reflects the affinity of the ***w***MNR particles towards Cd^{2+} ions[29]. Negative values of ΔG^0 (-3.88, -5.04 and -6.0 kJ mol^{-1} at 303, 313 and 323 K respectively) indicate spontaneous adsorption. The degree of spontaneity is found to be eased with increasing temperature.

Mechanism of Cd^{2+} sorption onto *w*MNR

It is widely accepted that the adsorption of heavy metals onto adsorbent surfaces involves various mechanisms such as electrostatic attraction/repulsion, chemical interaction and ligand-exchange. The adsorption mechanisms are often deduced from sorption kinetics and equilibrium data. Faster kinetics, like in present case, is attributed to chemical interaction/ion exchange mechanism of sorption. As apparent from Table 2, sorption of Cd^{2+} onto ***w***MNR follows pseudo second-order kinetics, indicating chemical interaction between adsorbent and adsorbate during sorption. However, it may not be rate controlling step for the sorption of Cd^{2+} onto ***w***MNR due to rapid rate of uptake. ΔH^0 between 5.0 and 100 kcal mol^{-1} (20.9–418.4 kJ mol^{-1}) is reported as energy of chemical reaction comparable to adsorption taking place by chemical reaction i.e. chemisorption[30]. The ΔH^0 value obtained in present work (28.3 kJ mol^{-1}) suggests chemisorption type uptake of Cd^{2+} on ***w***MNR. Moreover, values of energy of activation (48.18-65.14 kJ mol^{-1}) for temperature range 303–323 K also support the chemical interaction between Cd^{2+} and ***w***MNR surface. In addition to that chemical interaction may take place in association with diffusion occurring through the pores of the sorbent. The equilibrium sorption capacity also increases with temperature indicating involvement of chemical reactions as well as diffusion based interaction between adsorbate and adsorbent during adsorption[24,31]. The adsorption process on porous sorbents is generally described with four stages, and one or more of which may determine the rate of adsorption and amount of adsorption on the solid surface. Those stages are described as bulk diffusion, film diffusion, intraparticle diffusion and finally adsorption of the solute on the surface[32]. Generally, bulk diffusion and adsorption steps are assumed to be rapid and therefore not rate determining. The

adsorbent used in present studies (***w***MNR) has extensive range of pore sizes (0.18-52.9 nm), including micro-, meso- and macropores. Moreover, in aqueous system, macropores are hydrated and may act as meso- or micro-pores. This type of material gives rise to three-stage plot of q_t versus $t^{½}$, as shown in Fig. 4(b). The second stage in Fig. 4(a) can be attributed to the intraparticle diffusion[33]. The value of the intercept C in this stage of Fig. 4(b) also provides information related to the thickness of the boundary layer[34]. The increasing values of intercept with the rise in temperature suggest importance of surface diffusion at elevated temperatures (Table 4), which is presumably, due to the greater random motion associated with the increased thermal energy. Although, linear section supports involvement of intraparticle diffusion in Cd^{2+} adsorption onto ***w***MNR, deviation of curve from origin indicates role of another rate-limiting steps. The multilinearity (like in present case) in curves drawn between q_t and t are often attributed to involvement of two or more steps in adsorption kinetics[24,35]. Thus, it may be concluded that the sorption of Cd^{2+} on to ***w***MNR takes place via chemical interaction at interface occurring under diffusion gradient throughout the porous surface of leached manganese nodule residue.

Regeneration/desorption studies

Regeneration of an adsorbent by means of desorption is of crucial importance as it helps assessing the potential of sorbent for commercial application. Desorption study also helps to clarify the nature of the adsorption process. In present studies, desorption studies were carried out by in-situ desorption experiments[36]. The desorption of Cd^{2+} at ***p***H 2, 3, 4, and 5 are 79.80, 29.22, 11.59 and 3.09% respectively. The equilibrium Cd^{2+} after desorption experiment is found to decrease after ***p***H 5. The regeneration of ***w***MNR shows that adsorption of Cd^{2+} on to the ***w***MNR is a reversible process and regeneration via desorption can be achieved to reuse it.

Conclusion

The leached manganese nodule residue (***w***MNR) generated by reduction roast-ammonia leaching is found to be a potentially useful material for removal of aqueous cadmium. The uptake of Cd^{2+} increases with increasing its initial concentrations and equilibrium is attained after 30 min time irrespective of initial concentration. The regression coefficient value shows that the adsorption of Cd^{2+} on leached manganese nodule residue follows pseudo second-order kinetics. The adsorption data are fitted well into the Langmuir isotherm. The values of separation factor (R_L) calculated from isotherm data depicts favorable adsorption of cadmium. The Q^o i.e. maximum loading capacity value obtained from Langmuir data is found to be 32.23 mg g^{-1} at 303 K, which improves to 38.14 mg g^{-1} at 323 K. Activation energy and thermodynamic data suggest endothermic, spontaneous and chemisorption type uptake of Cd^{2+} onto ***w***MNR. The Cd^{2+} loaded ***w***MNR could be regenerated by desorption in acidic ***p***H (2-4) for further use in adsorption.

References

1 Hanaa M, Eweida S, Eweida A & Farag A, ***Proceedings ICEHM2000*** (Cairo University, Egypt)***,*** 2000, 542.
2 Koji N, Etsuko K, Yasushi O & Yasushi S, ***J BioMetals,*** 17 (2004) 581.
3 Swaddiwudhipong W, Mahasakpan P, Funkhiew T & Limpatanachote P, ***J Med Assoc Thailand,*** 93 (2010) 1217.
4 Holan Z R, Volesky B & Prasetyo I, ***J Biotechnol Bioeng,*** 41 (1993) 819.
5 Rao K S, Mohapatra M, Anand S & Venkateswarlu P, ***Int J Eng Sci Technol,*** 2 (2010) 81.
6 Jana R K, Pandey B D & Premchand, ***Hydromet,*** 53 (1999) 45.
7 Jana R K, Srikanth S, Pandey B D, Kumar V & Premchand, ***Met Mater Proc,*** 11 (1999) 133.
8 Das N N & Jana R K, ***J Colloid Interface Sci***, 293 (2006) 253.
9 Nakamato K, ***Infrared Spectra of Inorganic and Coordination Compounds***, Part B, 5th edn (John Wiley & Sons, New York), 1997.
10 Nour E M, Teleb S M, AL-Khsosy N A & Refat M S, ***Synth React Inorg Met-Org Chem,*** 27 (1997) 505.
11 Perin D D & Dempsy B, ***Buffers for pH and Metal ion Control*** (Chapman & Hall, London), 1974.
12 Martell A E & Smith R M, ***Critical Stability Constants (Inorganic Chemistry)***, Vol, IV (Plenum, NewYork), 1977.
13 Reed N E & Matsumoto M R, ***Sep Sci Technol,*** 28 (1993) 2179.
14 Bahrami S, Bassi A S & Yanful E, ***Can J Chem Eng,*** 77 (1999) 931.
15 Wang C C, Chang C Y & Chen C Y, ***Macromol Chem Phys,*** 202 (2001) 882.
16 Denizil A, Senel S, Alsancak G, ˝Uzman N T & Say R, ***React Funct Polym,*** 55 (2003) 121.
17 Delacour M L, Gailliez E, Bacquet M & Morcellet M, ***J Appl Polym Sci,*** 73 (1999) 899.
18 Taty-Costodes V C, Fauduet H, Porte C & Delacroix A, ***J Hazard Mater,*** 105 (2003) 121.
19 Memon S Q, Memon N, Shah S W, Khuhawar M Y & Bhanger M I, ***J Hazard Mater,*** 139 (2007) 116.
20 Ho Y S, ***Scientometrics,*** 59 (2004) 171.
21 Ho Y S, ***J Hazard Mater,*** 136 (2006) 681.
22 Weber W J (Jr) & Moris J C, ***Proceedings 1st International Conference on Water Pollution Research*** (Pergamon Press, Oxford), 1962, 231.
23 Boparai H K, Joseph M & O'Carroll D M, ***J Hazard Mater,*** 186 (2011) 458.

24 Wu F C, Tseng R L & Juang R S, ***Chem Eng J,*** 153 (2009) 1.
25 Unuabonah E I, Adebowale K O & Olu-Owolabi B I, ***J Hazard Mater,*** 144 (2007) 386.
26 Langmuir I, ***J Am Chem Soc***, 38 (1916) 2221.
27 Freundlich H M F, ***J Phys Chem***, 57 (1906) 385.
28 Foo K Y & Hameed B H, ***Chem Engg J,*** 156 (2010) 2.
29 Barkat M, Nibou D, Chearouche S & Mellah A, ***Chem Eng Process,*** 48 (2009) 38.
30 Unlu N & Ersoz M, ***J Hazard Mater*** B, 136 (2006) 272.
31 Hall K R, Eagleton L C, Acrivos A & Vermeulen T, ***Ind Eng Chem Fundam,*** 5 (1966) 212.
32 Chingombe P, Saha B & Wakeman R J, ***J Colloid Inter Sci,*** 302 (2006) 408.
33 Ho Y S, Ng J C Y & Mckay G, ***Separation Purification Methods***, 29(2) (2000) 189.
34 Kavitha D & Namasivayam C, ***Bioresour Technol,*** 98 (2007) 14.
35 Ozcan A, Ozcan A S & Gok O, ***Proceedings Hazardous Materials and Wastewater—Treatment, Removal and Analysis*** (Nova Science Publishers, New York) 2007.
36 Chakravarty S, Mohanty Ashok, Nag Sudha T, Upadhyay A K, Konar J, Sircar J K, Madhukar A & Gupta K K, ***J Hazard Mater,*** 173 (2010) 502.